Available online at www.sciencedirect.com

SciVerse ScienceDirect

Ceramics International 39 (2013) 7879–7889

CERAMICS INTERNATIONAL

www.elsevier.com/locate/ceramint

Preparation of $CaCu_3Ti_4O_{12}$ ceramics with low dielectric loss and giant dielectric constant by the sol–gel technique

Yanyan Li, Pengfei Liang, Xiaolian Chao, Zupei Yang*

Key Laboratory for Macromolecular Science of Shaanxi Province, School of Materials Science and Engineering, Shaanxi Normal University, Xi'an 710062, Shaanxi, PR China

Received 28 January 2013; received in revised form 13 March 2013; accepted 14 March 2013
Available online 22 March 2013

Abstract

$CaCu_3Ti_4O_{12}$ precursor powders were synthesized by the sol–gel process. The optimized processing parameters for the synthesis of precursor powders were as follows: the Ti concentration was 0.60 mol/L, the pH value of the sol was 1.58, and the aging time of the sol was 6 h. After sintering at 1100 °C for 15 h, the CCTO ceramics with the highest density and fine-grained microstructure were obtained, exhibiting outstanding dielectric properties: $\varepsilon' \approx 3.50 \times 10^4$ and $\tan\delta = 0.014$ (at 1 kHz). The low dielectric loss was attributed to the highest grain boundary resistance which significantly reduced the leakage current across grain boundaries. A broad dielectric relaxation peak was observed around 300 °C. The complex impedance spectroscopy analysis suggested that the obtained $CaCu_3Ti_4O_{12}$ ceramics were electrically heterogeneous, consisting of semiconducting grains and insulating grain boundaries. The calculated grain boundary resistance and grain resistance were 0.87 MΩ and 3.50 Ω, respectively.

Keywords: A. Sol–gel processes; B. X-ray methods; C. Impedance; C. Dielectric properties

1. Introduction

With the miniaturization of the microelectronic devices such as dynamic random access memory (DRAM) and multi-layer ceramic capacitors (MLCC) [1], high dielectric constant materials with good temperature stability and low dielectric loss are in high demand. In the last few decades, $CaCu_3Ti_4O_{12}$ (CCTO) system has attracted much interest because of its high and nearly temperature independent dielectric constant ($\sim 10^4$–10^5) in a wide temperature range from 100 to 600 K [2–5]. Unfortunately, the high dielectric loss ($\tan\delta > 0.05$ at 1 kHz) of CCTO has inevitably limited its practical applications [6,7]. A lot of work has been carried out to solve this large $\tan\delta$ problem. The results showed that this problem was very challenging [8–11].

As one of the wet chemical methods, sol–gel process has shown considerable advantages including excellent chemical stoichiometry, compositional homogeneity, and lower crystallization temperature due to the mixing of liquid precursors on the molecular level [12,13]. The method is considered to be efficient to obtain CCTO ceramics with lower dielectric loss. Sun et al. have reported the preparation of CCTO ceramics by the sol–gel route [14] with $\varepsilon' \sim 2$–4×10^4 and $\tan\delta \sim 0.04$ (at 1 kHz and room temperature). Somsack et al. reported a modified sol–gel process for the preparation of CCTO ceramics with lower $\tan\delta \sim 0.02$ at 1 kHz at room temperature [15]. However, there are limited literatures reporting the detailed synthesis conditions for CCTO precursor powders by the sol–gel method. Here it is expected that CCTO ceramics, through optimizing the synthesis conditions of precursors, may further improve dielectric properties.

In this work, CCTO precursor powders were prepared via the sol–gel method. The effects of synthesis parameters on the phase structure of CCTO precursor powders were detailly studied. The microstructure and dielectric properties of the CCTO ceramics were also reported. The possible origin of giant permittivity was discussed based on the complex impedance spectroscopy. The high-temperature dielectric relaxation behavior was also discussed. The relevant

*Corresponding author. Tel.: +86 29 8153 0718; fax: +86 29 8153 0702.
E-mail address: yangzp@snnu.edu.cn (Z. Yang).

0272-8842/$ - see front matter © 2013 Elsevier Ltd and Techna Group S.r.l. All rights reserved.
http://dx.doi.org/10.1016/j.ceramint.2013.03.049

mechanism of lower dielectric loss was investigated as well according to the resistance of grain boundaries.

2. Experimental procedure

$Ca(NO_3)_2 \cdot 4H_2O$ (99%), $Cu(NO_3)_2 \cdot 3H_2O$ (99%) and Ti $(OC_4H_9)_4$ (≥98.0%) were used to prepare the CCTO precursor powders. Glacial acetic acid was used as the chelating reagent. Firstly, an appropriate amount of $Ca(NO_3)_2 \cdot 4H_2O$ and Cu $(NO_3)_2 \cdot 3H_2O$ were dissolved in ethanol diluted with water to form solution 1. Meanwhile, $Ti(OC_4H_9)_4$ was immixed into ethanol to form solution 2, quickly with vigorously stirring on a magnetic stirrer, then CH_3COOH was added into solution 2 immediately. In this part, various Ti concentrations were obtained through mixing with the different volume of ethanol. Secondly, the two solutions were mixed into a beaker under stirring, and diluted nitric acid was dripped dropwise into the solution to adjust the pH to 1.06–1.77 to form a transparent sol. The sol was then aged for 4–12 h at room temperature. Finally, Precursor powders were obtained by drying the gel precursors at 120 °C followed by a calcination at 700 °C in air. The as-prepared powders were pressed into pellets of 15 mm diameter under 100 MPa pressure. CCTO ceramics were obtained by sintering the pellets at 1050 °C, 1070 °C, 1100 °C and 1120 °C for 5–20 h, respectively.

The phase structures of the sintered specimens were identified by X-ray diffraction (XRD, D/max-2550/PC, Rigaku, Japan) technique using Cu Kα radiation. The microstructures of the nature surface were observed by scanning electron microscopy (SEM, Quanta 200, Philips, Netherlands). An energy dispersive X-ray spectroscopy (EDS) attached to the SEM was used to analyze the chemical compositions. For the purpose of measuring the electric properties, both sides of the samples were coated by silver paste and fired at 840 °C to form electrodes. Dielectric dispersion and complex impedance were measured by Agilent 4294A impedance analyzer in a frequency range from 40 Hz to 110 MHz at room temperature. Temperature dependence of dielectric constant and loss was measured by a LCR meter (Agilent E4980A) from room temperature to 400 °C at 0.6, 1.0 and 1.4 kHz, respectively.

3. Results and discussion

3.1. Synthesis of CCTO precursor powders

The Ti concentration and pH value of the solution and aging time of the sol play important roles in the preparation of the precursor powders by the sol–gel process. The XRD patterns of the CCTO precursor powders prepared at different Ti concentrations are shown in Fig. 1(a). All the major CCTO diffraction peaks are indexed as the perovskite phase according to JCPDS #75-2188 [18]. In addition, secondary phases, like $CaTiO_3$, CuO and TiO_2, can also be detected. To further illuminate the detailed effects of Ti concentration on the phase structure of CCTO powder in a quantitative way, the optimum conditions can be approximately chosen by the degree of orientation illustrated by the relative coefficient I_i/I_{total} which is given by formula (1):

$$\frac{I_i}{I_{total}} = \frac{\sum(I_{220}+I_{422})}{\sum(I_{220}+I_{400}+I_{422}+I_{310}+I_{222}+I_{321}+I_{440})} \quad (1)$$

where I_{220}, I_{400}, I_{422}, I_{310}, I_{222}, I_{321} and I_{440} are the measured diffraction intensities of the major peaks, i.e. (2 2 0), (4 0 0), (4 2 2), (3 1 0), (2 2 2), (3 2 1) and (4 4 0), respectively. The two strong diffraction peaks of (2 2 0) and (4 2 2) are used to approximately assess the crystallinity of CCTO phase. The I_i/I_{total} as a function of Ti concentrations in CCTO powders calcined at 700 °C is shown in Fig. 1(b). It can be observed that the I_i/I_{total} reaches the highest value when the Ti concentration is 0.60 mol/L, indicating that the largest amount of CCTO phase can be obtained under this condition.

Fig. 2(a) shows the XRD patterns of the calcined CCTO precursors powders prepared with a Ti concentration of 0.60 mol/L at different pH values of the solutions. As is

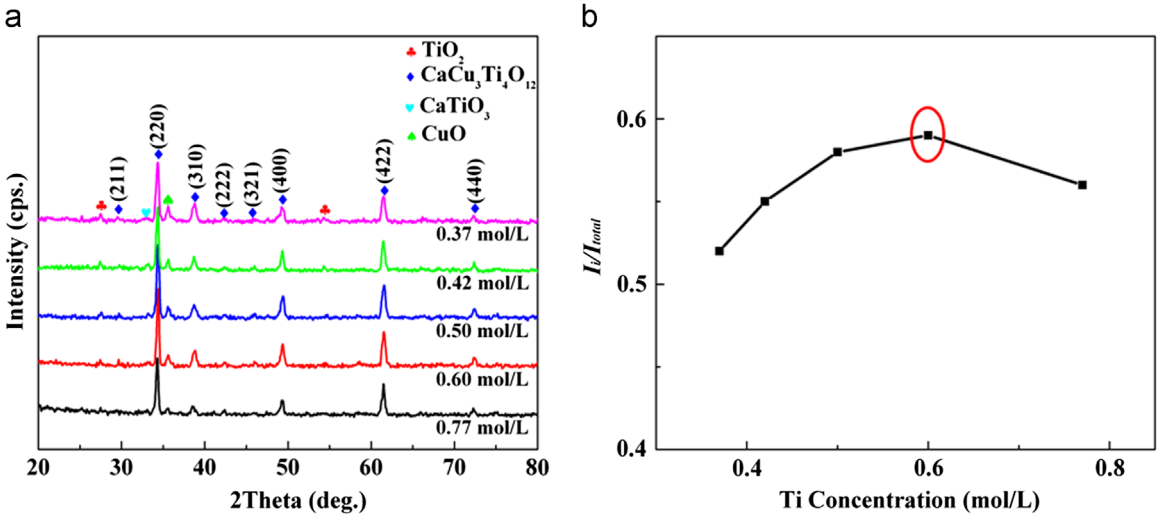

Fig. 1. (a) XRD patterns of the CCTO precursor powders prepared at different Ti concentrations. (b) I_i/I_{total} as a function of Ti concentration for CCTO powders calcined at 700 °C.

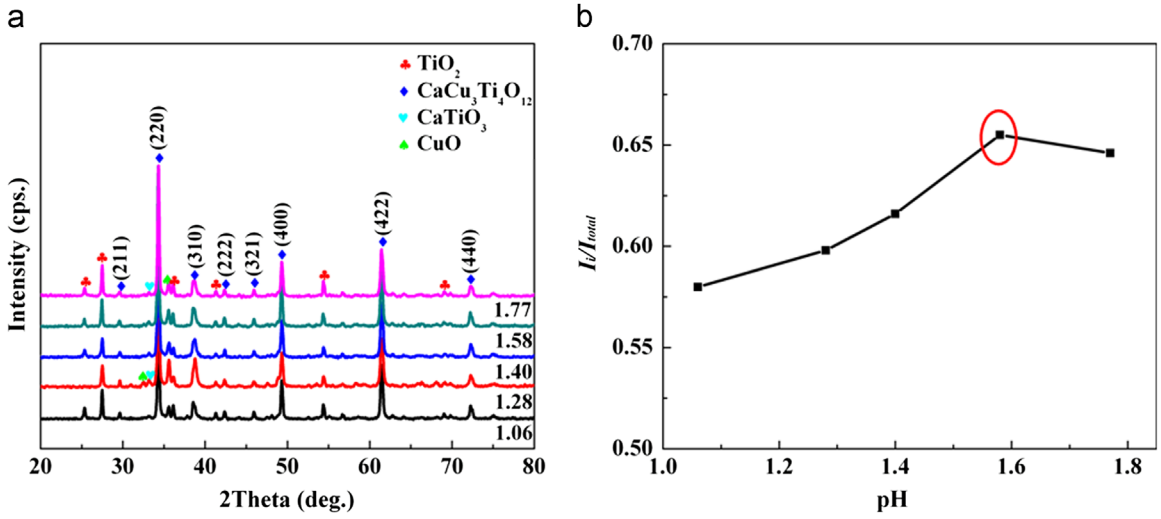

Fig. 2. (a) XRD patterns of the calcined CCTO precursors powders prepared with a Ti concentration of 0.60 mol/L at different pH values of the solutions. (b) I_i/I_{total} as a function of pH value for CCTO powders calcined at 700 °C.

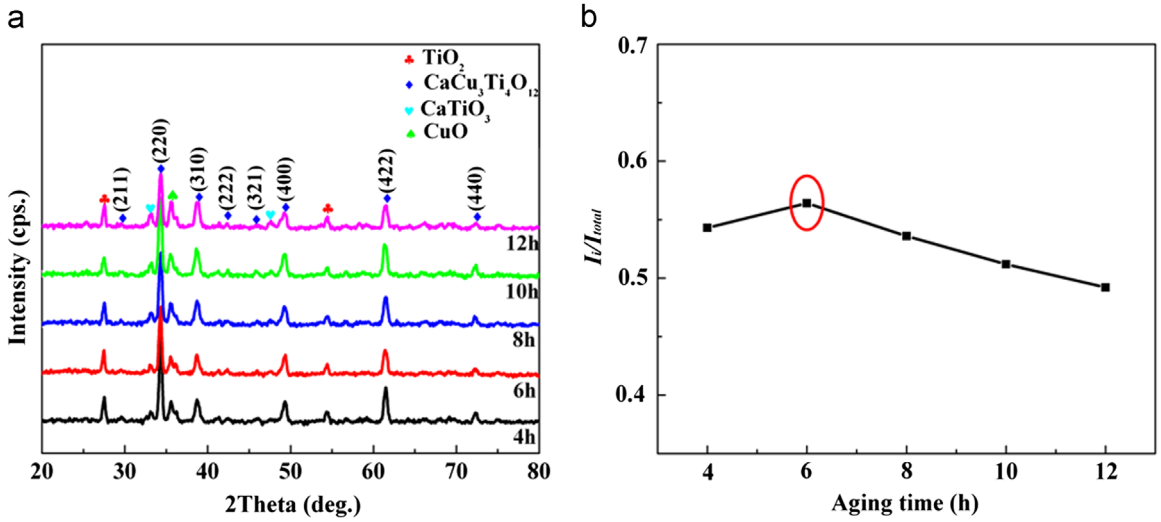

Fig. 3. (a) XRD patterns of the calcined CCTO precursor powders prepared at different aging time with a Ti concentration of 0.60 mol/L and pH value of 1.58. (b) I_i/I_{total} as a function of aging time for CCTO powders calcined at 700 °C.

shown in Fig. 2(a), all the major CCTO diffraction peaks are indexed as the perovskite phase according to JCPDS #75-2188. Secondary phases like $CaTiO_3$, CuO and TiO_2 can also be detected. According to Eq. (1), Fig. 2(b) demonstrates the I_i/I_{total} as a function of pH values to be used to prepare CCTO powders calcined at 700 °C. As can be found in Fig. 2(b), the I_i/I_{total} reaches the highest value when the pH value is 1.58.

The XRD patterns of the calcined CCTO precursor powders prepared at different aging time with Ti concentration of 0.60 mol/L and pH of 1.58 are displayed in Fig. 3(a). According to Fig. 3(a), all the major diffraction peaks can be indexed as a body centered cubic perovskite-related structure of space group *Im*3 according to JCPDS #75-2188. Additionally, $CaTiO_3$, CuO and TiO_2 can also be found. Fig. 3(b) shows the I_i/I_{total} as a function of aging time for CCTO powders calcined at 700 °C. As is shown in Fig. 3(b), the I_i/I_{total} reaches the highest value when the aging time is 6 h.

It can be concluded that the optimum parameters for the preparation of CCTO precursor powders by the sol–gel method are as follows: the Ti concentration is 0.60 mol/L, the pH value is 1.58 and the aging time is 6 h.

3.2. Phase structure and microstructure of CCTO ceramics

Fig. 4(a) and (b) show the typical X-ray diffraction patterns of CCTO ceramics sintered at different sintering temperatures for 5 h and sintered at 1100 °C for different holding times, respectively. According to Fig. 4, all the major diffraction peaks in the XRD patterns can be indexed as the body-centered cubic with the space group *Im*3 according to JCPDS #75-2188. A small amount of CuO and TiO_2 peaks can also be detected according to JCPDS #45-0937 and #21-1272. The presence of CuO phase is mainly due to Cu^{2+} diffusion from the inside to

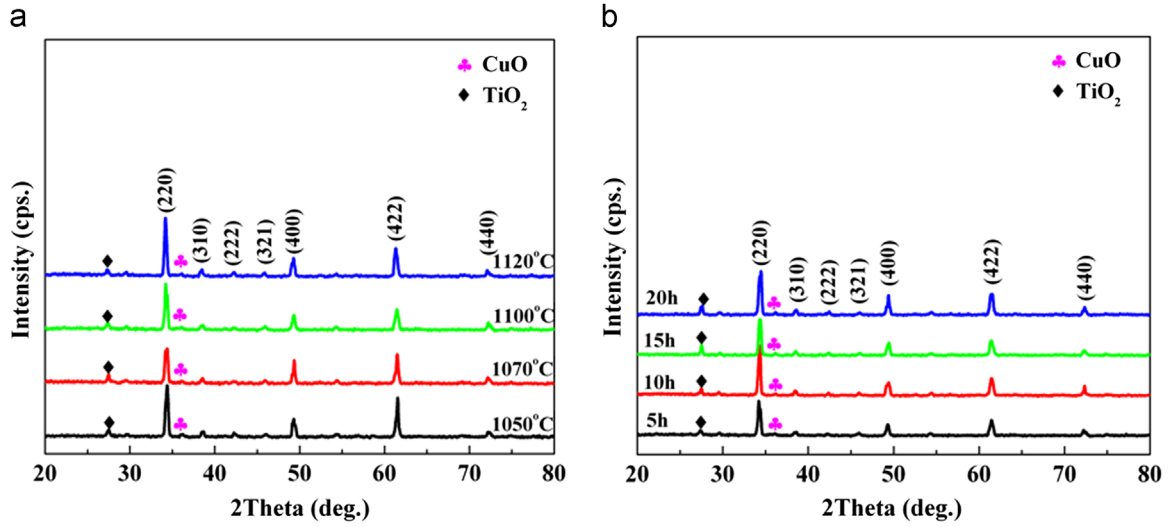

Fig. 4. (a) XRD patterns of CCTO ceramics sintered at different sintering temperatures for 5 h. (b) XRD patterns of CCTO ceramics sintered at 1100 °C for different holding times.

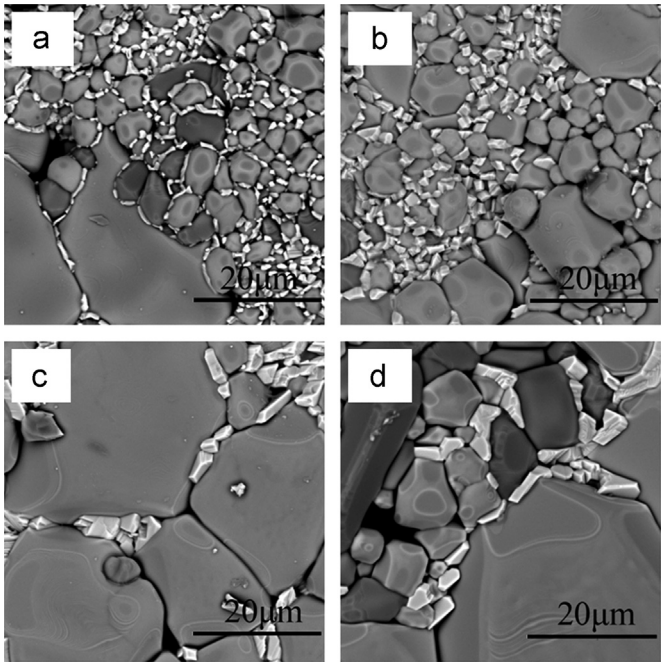

Fig. 5. The SEM photographs of the surface of CCTO ceramics sintered at different temperatures for 5 h: (a) 1050 °C, (b) 1070 °C, (c) 1100 °C and (d) 1120 °C.

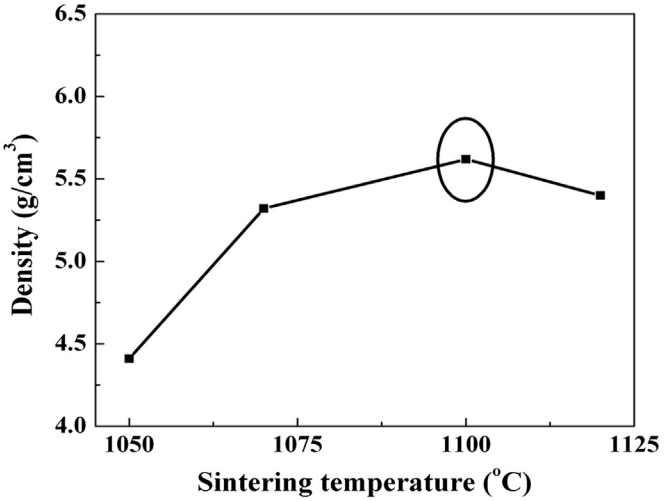

Fig. 6. Densification behavior as a function of sintering temperature for CCTO ceramics sintered for 5 h.

the surface of grains and oxygen missing from grain boundaries at high temperature during the sintering process [19].

Fig. 5 reveals the SEM photographs of the surface of CCTO ceramics sintered at 1050 °C, 1070 °C, 1100 °C and 1120 °C for 5 h, respectively. As is shown in Fig. 5, with increasing the sintering temperature, the grain size of the samples firstly increases and then decreases, while the porosity exhibits an opposite variation trend. When sintered at 1100 °C, a relatively homogeneous microstructure with clear grain boundaries and low porosity can be obtained. However, the microstructure becomes inhomogeneous and the porosity begins to increase at 1120 °C.

Densification behavior of CCTO ceramics sintered at different temperatures is shown in Fig. 6. With increasing sintering temperature, the density of the CCTO ceramics reaches to a maximum value of 5.62 g/cm^3 at 1100 °C. Further increasing the sintering temperature to 1120 °C causes a steep fall in the density, which is in agreement with the results obtained from Fig. 5.

The SEM micrographs of the samples sintered at 1100 °C for different holding time are shown in Fig. 7. With the increase of the holding time, the grain size firstly increases and then decreases, which may be caused by the existence of CuO second phase. It is known that a small amount of CuO can act

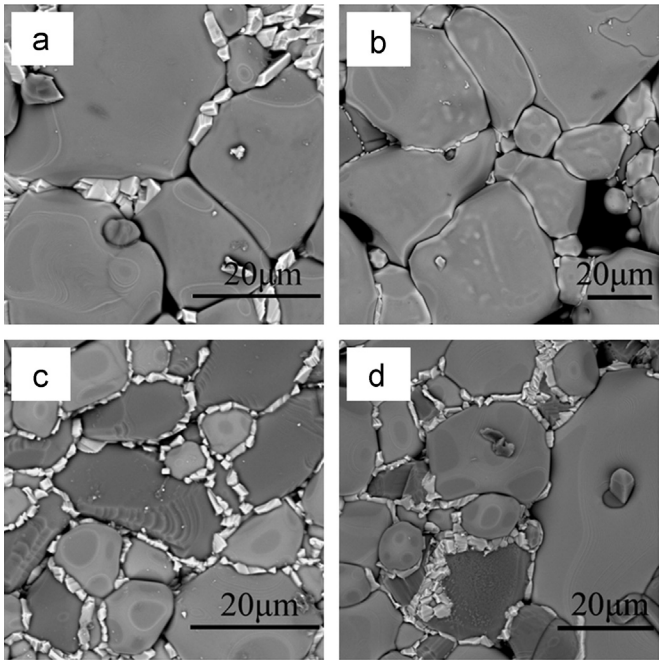

Fig. 7. The SEM photographs of the surface of CCTO ceramics sintered at 1100 °C for different holding times: (a) 5 h, (b) 10 h, (c) 15 h and (d) 20 h.

as a sintering aid for various ceramics (e.g. $BaTiO_3$-based ceramics) to promote the grain growth and ceramic densification due to its low melting point and liquid-phase effect [20–23]. The evaporation of CuO phase becomes more rapid with increasing sintering temperature, and then condenses around the grain boundaries at cooling stage, which could inhibit grain growth. To some extent, the CuO segregation effect is considered to play very important roles in the formation of the insulating grain boundaries and has a significant influence on ε' [24–28]. When sintered at 1100 °C for 15 h, the ceramics show relatively homogeneous microstructure with lower porosity, as is shown in Fig. 7(c). Further prolonging the holding time to 20 h, the samples show higher porosity and abnormal grain growth.

In order to further determine the unknown phase presented in Figs. 5 and 7, the EDS analysis is applied, and the results are shown in Fig. 8. Fig. 8(a) and (b) show the EDS spectrum obtained from the grain surface and grain boundary of CCTO ceramics sintered at 1100 °C for 15 h. The results indicate that the element mole ratio of the grain surface (a) is Ca:Cu:Ti = 1:3.33:4.38 which is nearly stoichiometric for $CaCu_3Ti_4O_{12}$; the element mole ratio of the grain boundary (b) is Ca:Cu:Ti = 1:45.71:8.86 indicating the existence of Cu-rich phase

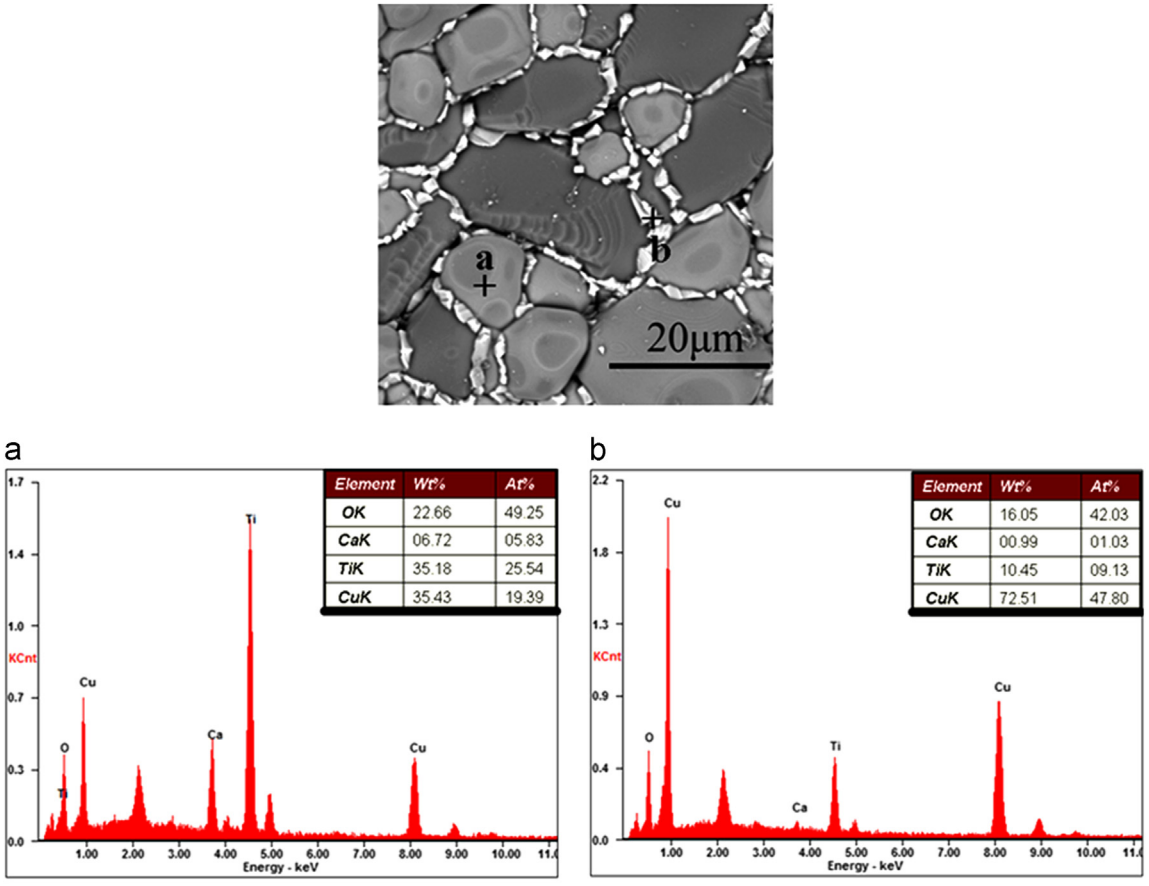

Fig. 8. The SEM photograph and EDS spectrum of the surface of CCTO ceramics sintered at 1100 °C for 15 h and EDS analysis pointed on the surface (a) and grain boundary (b).

in the grain boundaries region, which is in good agreement with the XRD analysis obtained in Fig. 4.

It is reported that the extrinsic defects, like grain boundaries and domain boundaries, perform as the insulating layer in ceramics which have great contributions to the giant permittivity phenomenon in CCTO ceramics [29–31]. Four defect relaxation behaviors are found in CCTO ceramics, which are attributed to the responses of grains, grain boundaries, domain boundaries and the migration of oxygen vacancies [32]. Furthermore, with respect to the formation of insulating grain boundaries, both segregation of Cu ions to grain boundaries and CuO located at triple-point sites bring out the formation of insulating grain boundaries [27,28]. The electron hopping between Cu^{+} and Cu^{2+} or Ti^{3+} and Ti^{4+} results in the formation of semiconducting grains in CCTO ceramics [23].

Fig. 9 presents the densification behavior as a function of holding time for CCTO ceramics sintered at 1100 °C. As is shown in Fig. 9, the density of CCTO samples increases with increasing the holding time. The density reaches the highest value of 6.52 g/cm^3 when the holding time is 15 h, which is in accordance with the results of Fig. 7(c). With further increasing the holding time, the density decreases. The samples with high density can be obtained when sintered at 1100 °C for 15 h.

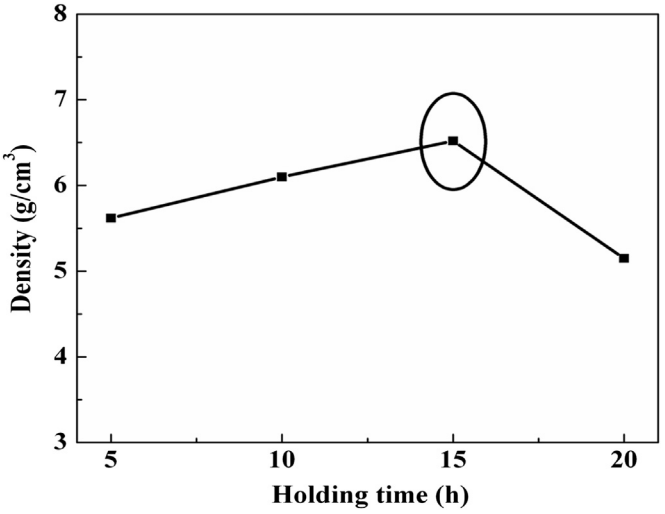

Fig. 9. Densification behavior as a function of holding time for CCTO ceramics sintered at 1100 °C.

3.3. Dielectric properties of CCTO ceramics

The frequency dependence of dielectric constant and dielectric loss at room temperature of the ceramics prepared at different sintering temperatures for 5 h is shown in Fig. 10(a). According to Fig. 10(a), all of the samples exhibit giant dielectric constant when the frequency is below 1 MHz. The values of dielectric constant for all samples are $> 10^4$ in the frequency range from 40 to 10^5 Hz. However, as the frequency increases to 1 MHz, the dielectric constant of all samples decreases rapidly and then inclines to a constant, which indicates a typical characteristic of Debye relaxation [33]. These results reveal that all samples have good frequency stability below 1 MHz. The dielectric behaviors of all samples are similar to the reported results [30]. Fig. 10(b) shows the dielectric constant and loss tangent as a function of sintering temperature for CCTO ceramics. As is shown in Fig. 10(b), the dielectric constant reaches the maximum value of 1.32×10^4 and the loss tangent reaches the minimum value of 0.051 (measured at 10 kHz) when the samples are sintered at 1100 °C for 5 h.

The frequency dependence of dielectric constant for samples prepared at 1100 °C with different holding times is shown in Fig. 11(a). According to Fig. 11(a), CCTO samples sintered at 1100 °C for 15 h exhibit the highest dielectric permittivity in low frequency region, and the dielectric constant sharply decreases to < 100 with increasing the frequency, showing a Debye-type relaxation [34,35]. The frequency dependence of dielectric loss for samples prepared at 1100 °C with different holding times is shown in Fig. 11(b). It can be clearly seen in the inset of Fig. 11(b) that the values of the dielectric loss are

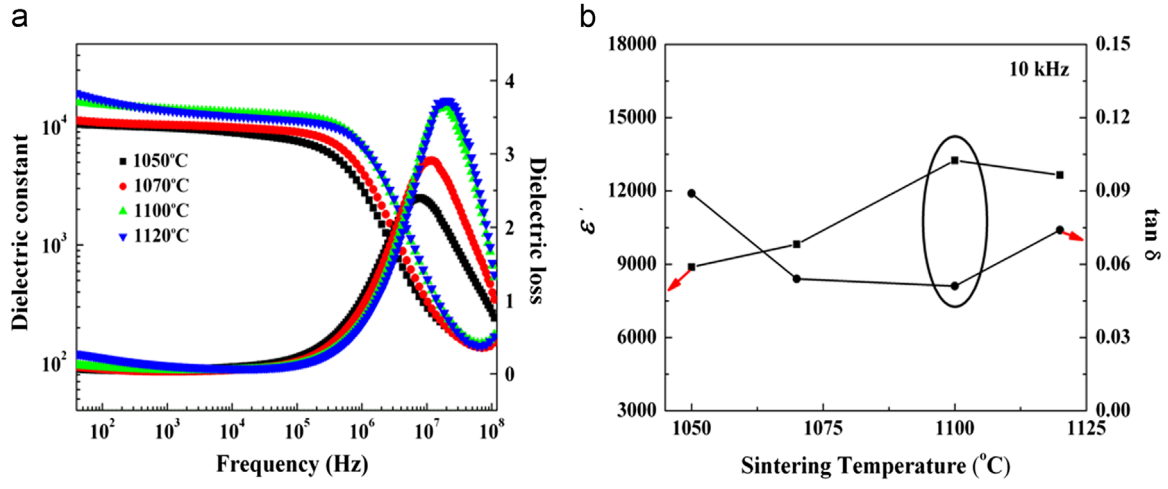

Fig. 10. (a) Frequency dependence of dielectric constant and dielectric loss measured at room temperature of CCTO ceramics sintered at different temperatures for 5 h. (b) Dielectric constant and loss tangent of CCTO ceramics as a function of sintering temperature for CCTO ceramics measured at 10 kHz.

lower than 0.04 in the frequency range from 40 to 10^4 Hz when the samples are sintered at 1100 °C for 15 h. Fig. 11(c) shows dielectric constant and loss tangent as a function of holding time for CCTO ceramics. As is shown in Fig. 11(c), the highest dielectric constant of 3.50×10^4 and lowest loss tangent of 0.014 of the CCTO ceramics are obtained when sintered at 1100 °C for 15 h (1 kHz), respectively. The results show that the dielectric constant of CCTO ceramics tends to increase significantly through increasing holding time and the tan δ tends to decrease gradually. The tan δ value herein is 0.014 and the ε' value is 3.50×10^4 (1 kHz), which are much more superior to those reported by Somsack et al. ($\varepsilon' = 9516$ and tan $\delta = 0.02$ at 1 kHz) [15]. According to Figs. 9 and 11, it is evidenced that CCTO ceramics with high density and excellent dielectric properties ($\varepsilon' \approx 3.50 \times 10^4$, tan $\delta = 0.014$ at 1 kHz) can be obtained from the samples sintered at 1100 °C for 15 h.

Fig. 12(a) and (b) demonstrate the temperature dependence of the dielectric constant (ε') and dielectric loss for CCTO samples sintered at 1100 °C for 15 h at 0.6, 1.0, and 1.4 kHz, respectively. The value of dielectric constant shows small variations with temperature and frequency in the temperature range from room temperature to ~120 °C. Further increasing temperature, $\varepsilon'(T)$ displays a steplike increase tendency to a higher value of about 1.50×10^5, which may be attributed to the interfacial relaxation process occurred at grain boundary in CCTO samples [23,36]. In addition, the corresponded small peaks in loss tangent shifted to higher temperatures as the frequency increases. Especially, as the temperature increases to ~300 °C, broad dielectric peaks appear and decrease in amplitude with increasing frequencies, which are accompanied by shift of small loss inflexions to high temperature with increasing frequencies, as shown in the inset of Fig. 12(b). Note that this broad dielectric relaxation peak is asymmetrical in geometry. It is known that the relaxation strength for the dipolar relaxation of defects in the lattice can be normally considered as a function of measured temperature, which is

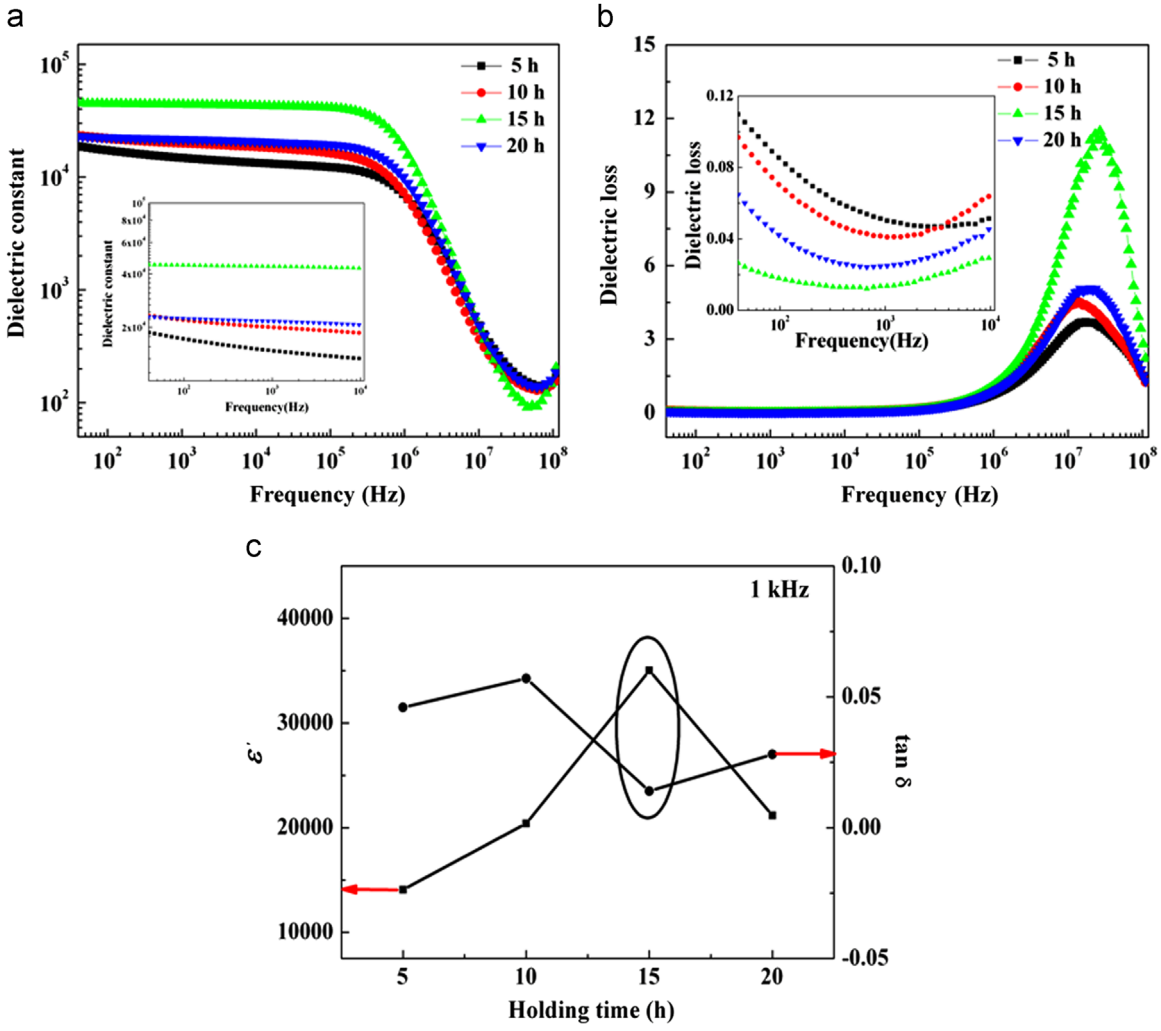

Fig. 11. (a) Frequency dependence of dielectric constant measured at room temperature for CCTO ceramics sintered at 1100 °C for different holding times. (b) Frequency dependence of dielectric loss measured at room temperature for CCTO ceramics sintered at 1100 °C for different holding times. The insets show the frequency dependence of dielectric loss measured at room temperature between 40 Hz and 10^4 Hz. (c) Dielectric constant and loss tangent as a function of holding time for CCTO ceramics measured at 1 kHz.

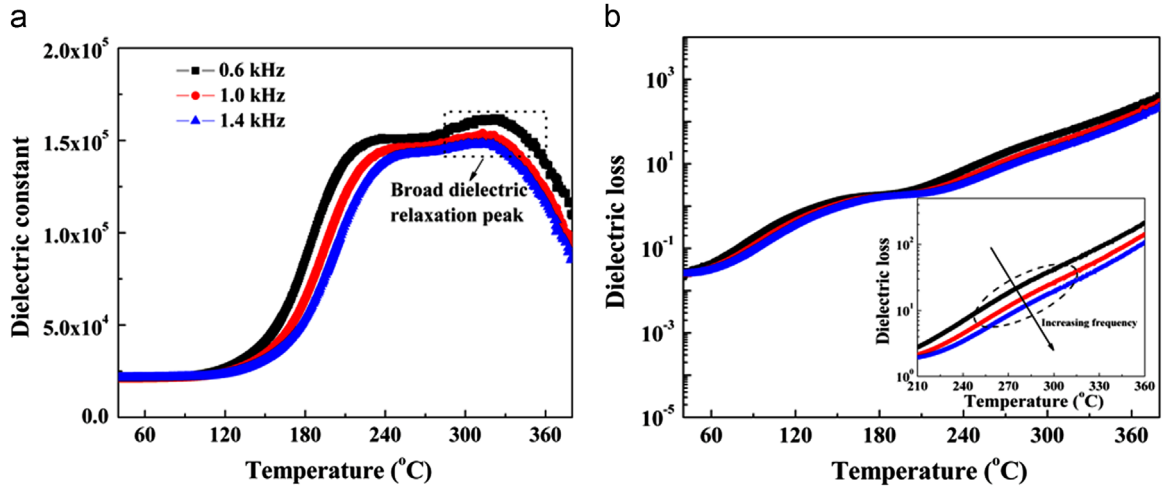

Fig. 12. (a) Temperature dependence of the dielectric constant for CCTO ceramics sintered at 1100 °C for 15 h at 0.6, 1.0 and 1.4 kHz. (b) Temperature dependence of the dielectric loss for CCTO ceramics sintered at 1100 °C for 15 h at 0.6, 1.0 and 1.4 kHz in the temperature range from 40 °C to 390 °C.

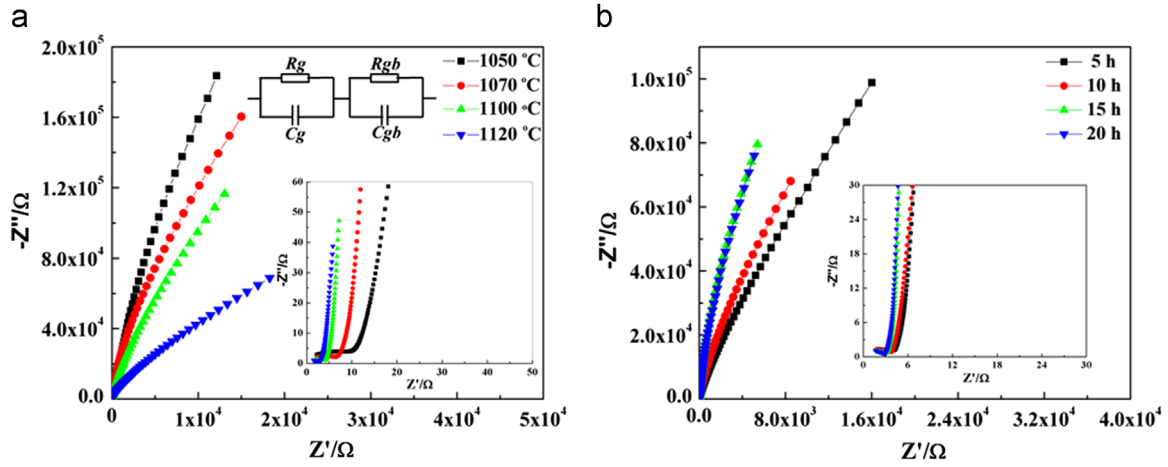

Fig. 13. (a) Impedance complex plane plots for CCTO ceramics sintered at different temperatures for 5 h. The inset shows the IBLC model equivalent circuit. (b) Impedance complex plane plots for CCTO ceramics sintered at 1100 °C for different holding times. The insets show an expanded view of high-frequency data close to the origin.

described with

$$\Delta\varepsilon = \varepsilon_s - \varepsilon_\infty = N\mu^2/3k_BT, \tag{2}$$

where ε_s is the static permittivity, ε_∞ is the permittivity at high frequency, N is the number of defect dipoles, and μ is the dipole moment [37]. It can be easily obtained from Eq. (2) that the relaxation strength of the dipolar relaxation of defects decreases inversely in proportion to the temperature. Therefore, this broad dielectric relaxation peak in our experiment may be attributed to the decrease of the dipolar relaxation of defects in CCTO lattice with increasing the temperature.

3.4. Complex impedance analysis

Fig. 13(a) and (b) show impedance spectroscopy of CCTO ceramics with different sintering temperatures and different holding times, respectively. The curves of all the samples show a single semicircular arc with a nonzero high frequency intercept, indicating that all CCTO ceramics should be electrically heterogeneous. The higher frequency response corresponding to the small arc is associated with the grains, and the lower one is attributed to the grain boundaries. These two semicircular arcs can be modeled as an equivalent circuit consisting of two parallel *RC* elements connected in series: one *RC* element, i.e. *RgCg*, represents the semiconducting grains, and the other, i.e. *RgbCgb*, represents the insulating grain boundary regions, as shown in the inset of Fig. 13(a). For such an equivalent circuit, each *RC* element ideally arises semicircular arc in complex impedance plane Z^* [38] described as follows:

$$Z^* = Z' - iZ'' \tag{3}$$

In AC circuits, for a pure resistor and capacitor, $Z^* = R$ and $1/i\omega C$, respectively. Therefore, the impedance can be

expressed as Eq. (4) for each *RC* element.

$$Z^* = \frac{1}{1/R + i\omega C} = \frac{R}{1 + i\omega RC} \tag{4}$$

In our experiment, the impedance spectrum can be modeled as two *RC* elements connected in series. Therefore, the complex impedance ($Z^* = Z' - iZ''$) here can be expressed as

$$Z' = \frac{R_g}{1 + (\omega R_g C_g)^2} + \frac{R_{gb}}{1 + (\omega R_{gb} C_{gb})^2} \tag{5}$$

and

$$Z'' = R_g \left[\frac{\omega R_g C_g}{1 + (\omega R_g C_g)^2} \right] + R_{gb} \left[\frac{\omega R_{gb} C_{gb}}{1 + (\omega R_{gb} C_{gb})^2} \right] \tag{6}$$

where R and C are the resistance and capacitance, respectively, the subscripts g and gb refer to the grains and grain boundaries, respectively, and ω is the angular frequency. Based on Eq. (6), the response peaks of the grains and the grain boundaries are located at $1/(2\pi R_g C_g)$ and $1/(2\pi R_{gb} C_{gb})$, respectively, and the peak value is proportional to the associated resistance. The above results demonstrate that CCTO ceramics are electrically heterogeneous, which is well consistent with the internal barrier layer capacitance (IBLC) model [39–41].

Fig. 14(a) and (b) show the calculated R_g and R_{gb} of the CCTO ceramics as a function of sintering temperature and holding time, respectively. As can be seen in Fig. 14(a), with increasing sintering temperature, the value of grain resistance (R_g) and grain boundaries resistance (R_{gb}) monotonically decrease. The decrease of the semiconducting grains resistance indicates that the formation of the semiconducting grains can be promoted through increasing the sintering temperature. It can be found in Fig. 14(b) that the resistance of grain boundary of the ceramics sintered for 15 h reaches the highest value of 0.87 MΩ, which leads to the lowest dielectric loss. Due to $R_{gb} \gg R_g$, $C_{gb} \approx C_p \gg C_g$ [38,42], and $\omega R_g C_{gb} \ll 1$ (at room temperature), one may easily derive the formula [9]

$$tan\delta = \frac{1}{\omega R_{gb} C_p} + \omega R_g C_p \tag{7}$$

where ω is the angular frequency. Obviously, the first term on the right of Eq. (7) is due to the grain boundary responses at low frequencies, while the second term is due to the bulk grain responses at high frequencies. The highest grain boundary resistance of the samples sintered at 1100 °C for 15 h is attributed to the largest amount of CuO segregation because CuO segregation is considered to play very important roles in the formation of the insulating grain boundaries [23,27,28]. Furthermore, as shown in Figs. 4 and 8(b), the presence of CuO segregation in our ceramics can be directly recognized by the XRD analysis and the EDS spectrum.

Fig. 15(a) shows the frequency dependence of dielectric loss of the CCTO ceramics respectively prepared by the sol–gel and solid state method between 40 Hz and 110 MHz. The inset of Fig. 15(a) shows the frequency dependence of dielectric loss measured at room temperature between 40 Hz and 100 kHz. It can be seen that the dielectric loss of CCTO ceramics prepared by the sol–gel method is much lower than that prepared by the solid state method in the frequency range from 40 Hz to 100 kHz. Furthermore, It is evident that the dielectric loss peak is located at a comparatively higher frequency when the ceramics are prepared by sol–gel method. In general, the higher the resistance of grain boundaries is, the lower the dielectric loss in the low frequency region is. Herein, it is assumed that the ceramics prepared by the sol–gel method possess lower grains resistance and higher grain boundaries resistance than those prepared by the solid state method. In order to verify this assumption on solid ground, the complex impedance data have been collected to obtain comprehensive electric details, which is shown in Fig. 15(b). It is clear that compared with the CCTO ceramics prepared by the solid state method, the ceramics prepared by the sol–gel method exhibit a lower grain resistance and a higher grain boundaries resistance. Therefore, it is concluded that the lower dielectric loss is attributed to the higher grain boundaries resistance.

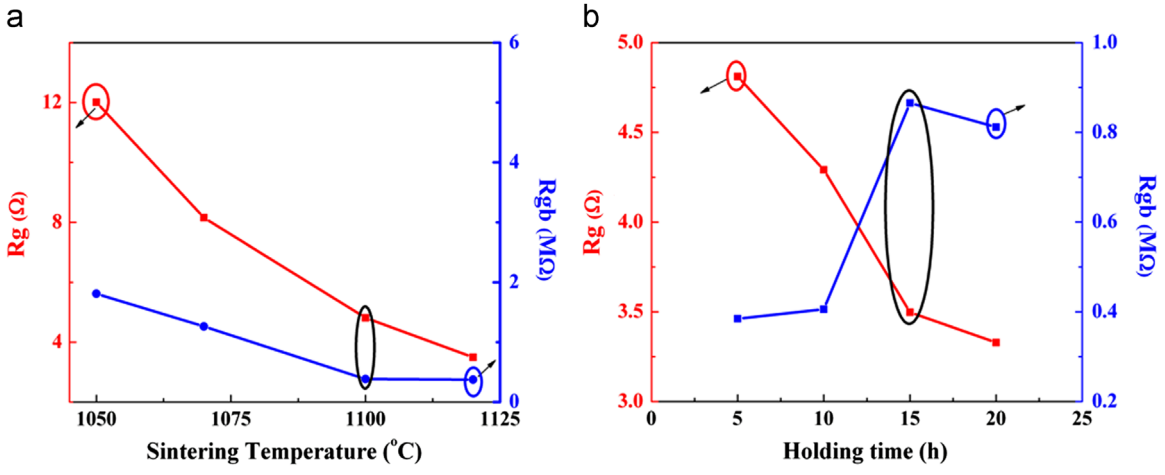

Fig. 14. (a) The calculated R_g and R_{gb} as a function of sintering temperature for CCTO ceramics. (b) The calculated R_g and R_{gb} as a function of holding time for CCTO ceramics.

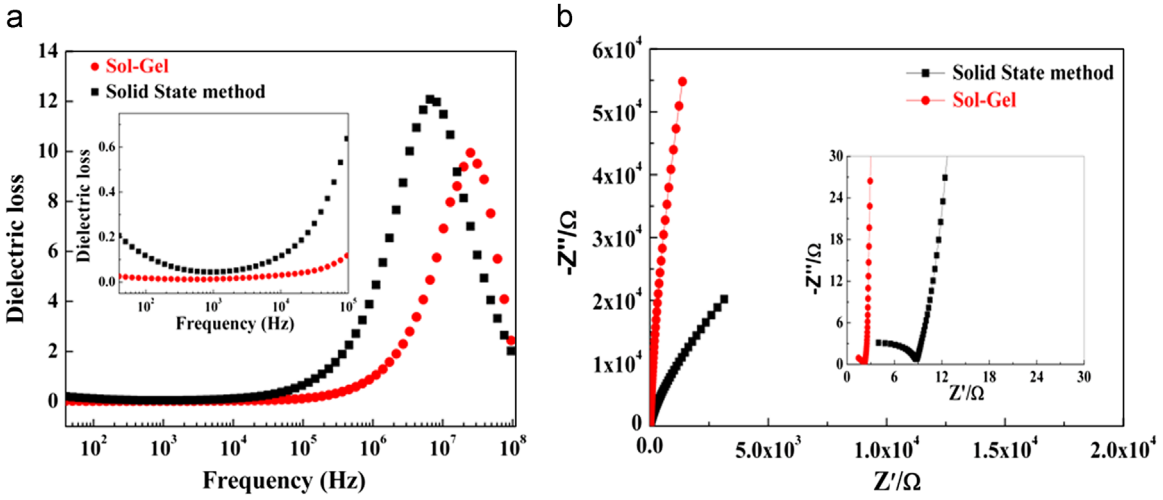

Fig. 15. (a) Frequency dependence of dielectric loss of the CCTO ceramics respectively prepared by the sol–gel and solid state method between 40 Hz and 110 MHz. The inset shows the frequency dependence of dielectric loss measured between 40 Hz and 100 kHz. (b) The complex impedance plots of CCTO ceramics prepared by the sol–gel and solid state method. The inset shows an expanded view of high-frequency data close to the origin.

4. Conclusions

The optimum synthesis parameters of the CCTO precursor powder had been firstly reported as follows: the Ti concentration was 0.60 mol/L, the pH value of the sol was 1.58, and the aging time to the sol was 6 h. CCTO ceramics with the lowest dielectric loss value of 0.014 at 1 kHz had been obtained. The highest grain boundary resistance resulted in the lowest dielectric loss in the low frequency region. In particular, a broad dielectric relaxation peak could be found around 300 °C, which might arise from the decrease of the relaxation strength for the dipolar relaxation of defects in the lattice with increasing the temperature. In addition, the complex impedance analysis indicated that CCTO ceramics were electrically heterogeneous, consisting of insulating grain boundaries and semiconducting grains, which was well consistent with the internal barrier layer capacitance (IBLC) model.

Acknowledgments

This work was supported by National Science Foundation of China (NSFC) (Grant No. 51172136 and 51107077), Graduate Student Innovation Fund of Shaanxi Normal University (Project No. 2012CXS028), the Fundamental Research Funds for the Central Universities (Program No. GK201101004) and Open Fund of Shaanxi Province Key Laboratory (Program no. 2010SYS-07).

References

[1] M.A. Subramanian, L. Dong, N. Duan, B.A. Reisner, A.W. Sleight, High dielectric constant in $ACu_3Ti_4O_{12}$ and $ACu_3Ti_3FeO_{12}$ phases, Journal of Solid State Chemistry 151 (2000) 323–325.

[2] A.R. West, T.B. Adams, F.D. Morrison, D.C. Sinclair, Novel high capacitance materials: -$BaTiO_3$: La and $CaCu_3Ti_4O_{12}$, Journal of European Ceramics Society 24 (2004) 1439–1448.

[3] C.H. Mu, P. Liu, Y. He, J.P. Zhou, H.W. Zhang, An effective method to decrease dielectric loss of $CaCu_3Ti_4O_{12}$ ceramics, Journal of Alloys and Compounds 471 (2009) 137–141.

[4] C.C. Homes, T. Vogt, S.M. Shapiro, S. Wakimoto, A.P. Ramirez, Optical response of high-dielectric-constant perovskite-related oxide, Science 293 (2001) 673–676.

[5] A.P. Ramirez, M.A. Subramanian, M. Gardel, G. Blumberg, D. Li, T. Vogt, S.M. Shapiro, Giant dielectric constant response in a copper-titanate, Solid State Communications 115 (2000) 217–220.

[6] J.C. Zhao, J. Liu, G. Ma, Preparation, characterization and dielectric properties of $CaCu_3Ti_4O_{12}$ ceramics, Ceramics International 38 (2012) 1221–1225.

[7] F. Amaral, L.C. Costa, M.A. Valente, F. Henry, Dielectric relaxation and morphologic properties of $CaCu_3Ti_4O_{12}$ doped with GeO_2, Journal of Non-Crystalline Solids 355 (2009) 2160–2164.

[8] F. Amaral, L.C. Costa, M.A. Valente, Decrease in dielectric loss of $CaCu_3Ti_4O_{12}$ by the addition of TeO_2, Journal of Non-Crystalline Solids 357 (2011) 775–781.

[9] L.X. Feng, X.M. Tang, Y.Y. Yan, X.Z. Chen, Z.K. Jiao, G..H. Cao, Decrease of dielectric loss in $CaCu_3Ti_4O_{12}$ ceramics by La doping, Physica Status Solidi (a) 203 (2006) 22–24.

[10] E.A. Patterson, S. Kwon, C.C. Huang, D.P. Cann, Effects of ZrO_2 additions on the dielectric properties of $CaCu_3Ti_4O_{12}$, Applied Physics Letters 87 (2005) 182911.

[11] L. Fang, M.R. Shen, W.W. Cao, Effects of postanneal conditions on the dielectric properties of $CaCu_3Ti_4O_{12}$ thin films prepared on Pt/Ti/SiO_2/Si substrates, Journal of Applied Physics 95 (2004) 6483–6485.

[12] C.J. Brinker, G.W. Scherer, The Physics and Chemistry of Sol–gel Processing, Academic Press, New York, 1990.

[13] Y.G. Metlin, Y.D. Tretyakov, Chemical routes for preparation of oxide high-temperature superconducting powders and precursors for superconductive ceramics, coatings and composites, Journal of Materials Chemistry 4 (1994) 1659–1665.

[14] D.L. Sun, A.Y. Wu, S.T. Yin, Structure, properties, and impedance spectroscopy of $CaCu_3Ti_4O_{12}$ ceramics prepared by sol–gel Process, Journal of the American Ceramic Society 91 (2008) 169–173.

[15] S. Vangchangyia, E. Swatsitang, P. Thongbai, S. Pinitsoontorn, T. Yamwong, S. Maensiri, V. Amornkitbamrung, P. Chindaprasirt, Very low loss tangent and high dielectric permittivity in pure-$CaCu_3Ti_4O_{12}$ ceramics prepared by a modified sol–gel process, Journal of the American Ceramic Society 95 (2012) 1497–1500.

[18] W.Q. Ni, X.H. Zheng, J.C. Yu, Sintering effects on structure and dielectric properties of dielectrics $CaCu_3Ti_4O_{12}$, Journal of Materials Science 42 (2007) 1037–1041.

[19] Q.L. Zhang, T. Li, Z.P. Chen, R.Z. Xue, Y.Q. Wang, The non-ohmic and dielectric behavior evolution of $CaCu_3Ti_4O_{12}$ after heat treatments in oxygen-rich atmosphere, Materials Science and Engineering B 177 (2012) 168–172.
[20] B.A. Bender, M.-J. Pan, The effect of processing on the giant dielectric properties of $CaCu_3Ti_4O_{12}$, Materials Science and Engineering B 117 (2005) 339–347.
[21] C.F. Yang, L. Wu, T.S. Wu, Effect of CuO on the sintering and dielectric characteristic of $(Ba_{1-x}Sr_x)(Ti_{0.9}Zr_{0.1})O_3$ ceramics, Journal of Materials Science 27 (1992) 6573–6578.
[22] P. Zheng, J.L. Zhang, S.F. Shao, Y.Q. Tan, C.L. Wang, Piezoelectric properties and stabilities of CuO-modified $Ba(Ti,Zr)O_3$ ceramics, Applied Physics Letters 94 (2009) 032902.
[23] P.F. Liang, Z.P. Yang, X.L Chao, Z.H. Liu, Giant dielectric constant and good temperature stability in $Y_{2/3}Cu_3Ti_4O_{12}$ ceramics, Journal of American Ceramics Society 95 (2012) 2218–2225.
[24] T.T. Fang, H.K. Shiau, Mechanism for developing the boundary barrier layers of $CaCu_3Ti_4O_{12}$, Journal of American Ceramics Society 87 (2004) 2072–2079.
[25] D. Capsoni, M. Bini, V. Massarotti, G. Chiodelli, M.C. Mozzati, C. B. Azzoni, Role of doping and CuO segregation in improving the giant permittivity of $CaCu_3Ti_4O_{12}$, Journal of Solid State Chemistry 177 (2004) 4494–4500.
[26] T.T. Fang, L.T. Mei, H.F. Ho, Effects of the Cu Stoichiometry on the microstructures, barrier-Layer structures, electrical conduction, dielectric responses, and stability of $CaCu_3Ti_4O_{12}$, Acta Materialia 54 (2006) 2867–2875.
[27] W.T. Hao, J.L. Zhang, Y.Q. Tan, W.B. Su, Giant dielectric-permittivity phenomena of compositionally and structurally $CaCu_3Ti_4O_{12}$-like oxide ceramics, Journal of American Ceramics Society 92 (2009) 2937–2943.
[28] W.T. Hao, J.L. Zhang, Y.Q. Tan, M.L. Zhao, C.L. Wang, Giant dielectric permittivity properties and relevant mechanism of $NaCu_3Ti_3SbO_{12}$ ceramics, Journal of the American Ceramic Society 94 (2011) 1067–1072.
[29] T.B. Adams, D.C. Sinclair, A.R. West, Characterization of grain boundary impedances in fine- and coarse-grained $CaCu_3Ti_4O_{12}$ ceramics, Physical Review B 73 (2006) 094124.
[30] J.L. Zhang, P. Zheng, C.L. Wang, M.L. Zhao, J.C. Li, J.F. Wang, Dielectric dispersion of $CaCu_3Ti_4O_{12}$ ceramics at high temperatures, Applied Physics Letters 87 (2005) 142901.
[31] J.Y. Li, X.T. Zhao, S.T. Li, M.A. Alim, Intrinsic and extrinsic relaxation of $CaCu_3Ti_4O_{12}$ ceramics: effect of sintering, Journal of Applied Physics 108 (2010) 104104.
[32] J.Y. Li, X.T. Zhao, F. Gu, M.A. Alim, Defects and dc electrical degradation in $CaCu_3Ti_4O_{12}$ ceramics: role of oxygen vacancy migration, Applied Physics Letters 100 (2012) 202905.
[33] H. Birey, Dielectric properties of aluminum oxide films, Journal of Applied Physics 49 (1978) 2898–2904.
[34] S.M. Moussa, B.J. Kennedy, Structural studies of the distorted perovskite $Ca_{0.25}Cu_{0.75}TiO_3$, Materials Research Bulletin 36 (2001) 2525–2529.
[35] R.N. Choudhary, U. Bhunia, Structural, dielectric and electrical properties of $ACu_3Ti_4O_{12}$ (A=Ca, Sr and Ba), Journal of Materials Science 37 (2002) 5177–5182.
[36] J.Y. Li, X.T. Zhao, F. Gu, S.T. Li, Defects and dc electrical degradation in $CaCu_3Ti_4O_{12}$ ceramics: role of oxygen vacancy migration, Applied Physics Letters 100 (2012) 202905.
[37] B.S. Kang, S.K. Choi, Diffuse dielectric anomaly of $BaTiO_3$ in the temperature range of 400–700 °C, Solid State Communications 121 (2002) 441–446.
[38] D.C. Sinclair, T.B. Adams, F.D. Morrison, A.R. West, $CaCu_3Ti_4O_{12}$: one-step internal barrier layer capacitor, Applied Physics Letters 80 (2002) 2153–2155.
[39] J. Li, A.W. Sleight, M.A. Subramanian, Evidence for internal resistive barriers in a crystal of the giant dielectric constant material: $CaCu_3Ti_4O_{12}$, Solid State Communications 135 (2005) 260–262.
[40] Z.P. Yang, L.J. Zhang, X.L. Chao, L.R. Xiong, J. Liu, High permittivity and low dielectric loss of the $Ca_{1-x}Sr_xCu_3Ti_4O_{12}$ ceramics, Journal of Alloys and Compounds 509 (2011) 8716–8719.
[41] H.M. Ren, P.F. Liang, Z.P. Yang, Processing, dielectric properties and impedance characteristics of $Na_{0.5}Bi_{0.5}Cu_3Ti_4O_{12}$ ceramics, Materials Research Bulletin 45 (2010) 1608–1613.
[42] W. Kobayashi, I. Terasaki, $CaCu_3Ti_4O_{12}/CaTiO_3$ composite dielectrics: Ba/Pb-free dielectric ceramics with high dielectric constants, Applied Physics Letters 87 (2005) 032902.